Chaotic mixing deep in the lung

Akira Tsuda*†, Rick A. Rogers*, Peter E. Hydon‡, and James P. Butler*

*Physiology Program, Harvard University, Boston, MA 02115; and ‡Department of Mathematics and Statistics, University of Surrey, Surrey GU2 7XH, United Kingdom

Communicated by Ewald R. Weibel, University of Bern, Bern, Switzerland, May 24, 2002 (received for review March 25, 2002)

Our current understanding of the transport and deposition of aerosols (viruses, bacteria, air pollutants, aerosolized drugs) deep in the lung has been grounded in dispersive theories based on untested assumptions about the nature of acinar airflow fields. Traditionally, these have been taken to be simple and kinematically reversible. In this article, we apply the recently discovered fluid mechanical phenomenon of irreversible low-Reynolds number flow to the lung. We demonstrate, through flow visualization studies in rhythmically ventilated rat lungs, that such a foundation is false, and that chaotic mixing may be key to aerosol transport. We found substantial alveolar flow irreversibility with stretched and folded fractal patterns, which lead to a sudden increase in mixing. These findings support our theory that chaotic alveolar flow—characterized by stagnation saddle points associated with alveolar vortices—governs gas kinematics in the lung periphery, and hence the transport, mixing, and ultimately the deposition of fine aerosols. This mechanism calls for a rethinking of the relationship of exposure and deposition of fine inhaled particles.

Pathogenic aerosols play a major role in causing or exacerbating many pulmonary diseases such as lung cancer, bronchitis, emphysema, and asthma (1–4) and in spreading infectious diseases such as influenza, anthrax, and tuberculosis (5–8). The long-term effects of particulate air pollution on public health are striking; they have been shown to be equivalent to a shortening of life expectancy of approximately 2 years in the United States (9, 10). The magnitude of this effect is comparable to the deaths caused by all cancers (11). Fine particles—less than a few micrometers in diameter—are of great concern because they can penetrate deep into the pulmonary acinus (i.e., the gas exchange region of the lung). The critical factor that determines the fate of inhaled fine particles—whether deposited deep in the lung or exhaled in the next breath—is the kinematic interaction of inhaled and residual alveolar gas, but the underlying mechanism of this interaction is still not well understood.

Because gas flow in the alveolar region occurs at very low Reynolds number (12) and the wall motion of the lung during breathing is essentially reversible (13–16), it has long been assumed that flow patterns deep in the lung are well described as a kinematically reversible Stokes flow (17–21). This means that, apart from the effects of molecular diffusion, a fluid "particle" that is transported by Stokes flow returns [by reversing the flow (22)] to its original position at the completion of one breathing cycle. This assumption implies that there is negligible flow-induced mixing between inhaled particles and the alveolar residual gas (17–21) and consequently little deposition of fine particles (18, 21). Experimental studies, however, consistently demonstrate appreciable aerosol mixing (23, 24) and deposition (25) deep in the lung, which cannot be accounted for by any known mechanism such as inertial streamline crossing, gravitational sedimentation, or diffusion within the context of reversible acinar flow. These unresolved basic contradictions between predictions and experimental observations necessitate a re-examination of our current understanding and a new approach to the identification of causal links between aerosol exposure and its health effects.

Our approach is based on two findings. First, our numerical simulations (26–28), performed to quantify the influence of structural characteristics of the acinar airways and the effects of cyclic expansion of the alveolated duct during normal breathing, showed complex acinar flow patterns. In particular, stagnation saddle points were noticed near the alveolar openings that are associated with slow alveolar recirculation. Lagrangian tracking of fluid particles indicated that the fluid motion exhibited unpredictable and irreversible stretched and folded patterns (26–28), characteristic of chaotic flow (29). Second, it has recently been discovered that oscillatory Stokes flow can exhibit chaotic behavior, which is therefore irreversible (30, 31). These two observations led us to hypothesize that chaotic flow can occur in the rhythmically expanding and contracting alveolated duct structure and that this can result in flow-induced aerosol mixing and deposition deep in the lung. The objective of the current study was to test this hypothesis by performing flow visualization experiments in excised animal lungs and to improve our understanding of the kinematic interaction of inhaled tidal air and residual alveolar gas deep in the pulmonary acinus.

Materials and Methods

To experimentally demonstrate how inhaled tidal air and residual alveolar gas interact, we used a flow visualization technique. Using ultra-low viscosity polymerizable fluids of two colors (one color representing tidal fluid, and the other the residual fluid), excised rat lungs were ventilated at very low Reynolds number flow conditions. Ventilation was halted at predetermined time points in the ventilatory cycle, and the fluids were polymerized. The detailed convective flow patterns were preserved in the casts; we examined these on lung sections by light microscopy and analyzed them as described below.

Working Fluids. The criteria we used in choosing these fluids were that (*i*) they are Newtonian—-similar to air during normal breathing—while the lungs are ventilated, and (*ii*) at a predetermined time they polymerize, thus preserving the flow patterns formed in fluid state. Rheological measurements (Polymer Fluid Lab, Massachusetts Institute of Technology) showed that the viscosity of our fluids (Microfil, Flowtech, Carver, MA) remained essentially constant ($\approx$15cP) with respect to shear rate (rate 15–500 sec^{-1}) and time (up to 30–40 min), confirming Newtonian behavior throughout the first phase (ventilation) of experiments (<20 min). Curing agent as specified by Microfil was added immediately before the start of each experiment, and rheological measurements provided evidence that the fluids did not change their Newtonian properties up to about 60 min, but after this time rapid curing occurred. Note also that the two fluids are made of the same material and therefore have negligible interfacial tension. Furthermore, they have very low viscosity; they flow easily in the acinar airways and convectively interact with each other under low Reynolds number flow conditions in a manner that, as argued below, approximates the kinematics of acinar flow during air breathing.

To exclude the possibility that any apparent mixing might be caused by intrinsic interface instability, control experiments were carried out. Two identical straight circular pipes with an inner diameter of 0.32 cm and a length of 100 cm were first filled with white fluid, followed by a slow injection of blue fluid in one pipe and a slow injection and withdrawal of blue fluid in the other. Stroke

Abbreviation: CV, coefficient of variation.

†To whom reprint requests should be addressed. E-mail: atsuda@hsph.harvard.edu.

volume was 2.2 ml. The fluids were allowed to polymerize, and the resulting interface pattern in the cast was examined.

Ventilation Conditions to Match Air Breathing Conditions. During quiet air breathing in normal adult humans, the flow distribution is dominated by the distribution of lung elastic recoil, because breathing periods are significantly longer than the lung's typical time constants (product of airway resistance and lung compliance). We matched these conditions in the excised rat lungs by increasing the ventilatory periods by a factor of 1,000, corresponding to the roughly 1,000-fold increase in viscosity of the fluid over that of the air. This matching also preserves local distending pressures throughout the lung.

Animals, Excised Lung Preparation. Adult Sprague–Dawley rats (approximately 300 g) were euthanized with an i.p. injection of sodium pentobarbital (100 mg/kg). This method of euthanasia is approved by the Harvard University Standing Committee on Animals. The lungs were excised and the trachea was cannulated. The lungs were degassed and placed in a chamber filled with saline with specific gravity nearly matching that of the working fluid. The chamber was connected to a piston pump volume ventilator (a 300-ml syringe and Harvard pump).

Flow Visualization Protocol. The excised rat lungs suspended in saline solution were first filled with white fluid to total lung capacity (TLC: 12 ml/300 g body mass), then deflated to 60% TLC. The lungs were then ventilated slowly with blue fluid, representing the tidal gas (tidal volume: 20% TLC), by cycling pleural pressure. Typical breathing period was 5 min. As noted above, except for the colors, the two fluids were essentially identical and remained Newtonian throughout the entire duration of the ventilation (<20 min), and physiologic pressures and flow distribution were preserved. To avoid irreversibility in the flow field caused by fluid inertia, we maintained low Reynolds number flow conditions ($Re \ll 1$) throughout the lung, including the large airways. Ventilation was continued for $N = 1$, 2, 3, or 4 cycles, with fresh tidal "blue" fluid for each breath. For each N, the ventilation was terminated at the end of expiration, and the lungs were held motionless to start polymerization of the compounds. This process took about 60 min. After the cast was dried at room temperature overnight, the lung cast was preserved in 2% glutaraldehyde in PBS (pH 7.4) for later analyses.

Microscopic Analysis and Data Collection. The mixing (interface) patterns of the two colors were examined on lung sections. The casts of the conducting airways and the first few acinar ducts (≈500 μm diameter) were isolated by following a representative airway path from the trachea to the right lower lobe. The airways and acinar ducts were cut generation by generation with a razor blade under dissection microscope to examine flow patterns on both transverse and longitudinal cross sections. The casts of lung parenchyma region were sliced at 500 μm thickness with a vibratome. The lung sections were examined by light microscopy with a video camera assembly (Nikon Microphot-FX, Sony DXC-755, ×20–80 magnification).

Results

Kinematic interaction between inhaled and residual alveolar fluid in rat lungs was visualized by using polymerizable Newtonian fluids of two colors. In our analysis, two different approaches were taken. (*i*) At a given time point $N = 1$, the flow patterns at different locations along the airway tree were examined. Airways of representative pathways were sampled generation by generation from the trachea to small airways of ≈500 μm in diameter. This approach allowed us to systematically study spatial variations in flow patterns generation by generation. (*ii*) To investigate the time course of acinar flow mixing, we focused on flow patterns at a given location of the acinar airways at four different time points ($N = 1$, 2, 3, or 4 cycles). In these studies, we randomly sampled alveolar ducts with approximately 200-μm diameter on lung sections and took the statistical averages of the image parameters at each N.

Stretch and Fold Mixing Patterns Observed at $N = 1$. After only one breathing cycle, remarkably complex stirring patterns emerged on transverse cross sections of the airways (Fig. 1). Stretch and fold patterns of the blue/white interface were observed throughout many airway generations, from the trachea down to the 12–13th generation (the most distal airways we examined for this analysis). The entire transverse cross section of the trachea (A1) was filled with myriad extremely fine blue/white striations, which formed convoluted swirling patterns. Similar patterns were seen on the transverse cross sections of the main stem bronchi (A2). This pattern was consistently seen through the eighth (A8), and even up to the 12th-generation (A12) airways (counted from the trachea). In contrast, the longitudinal airway sections showed much simpler patterns, displaying fine laminae of blue and white striations (see A7 for example; also tested at several other locations). The fact that there were very few complex patterns observed on the longitudinal sections suggests that inertia-based secondary flows such as turbulent eddies were not generated in this experiment.

The results of the control experiments in straight pipes showed little kinematic irreversibility. In the injection only experiment, the blue/white color interface was stretched to a parabolic tongue with a length/diameter ratio of 170 (data not shown). The tip of the tongue was located approximately twice as distal as the stroke length of bulk mean volume, suggesting that the flow in the pipe faithfully obeyed Poiseuille's Law. In injection and withdrawal experiment, after flow reversal this largely stretched color interface returned to its initial configuration with very little evidence of mixing.

Fractal Analysis of the Color Patterns. To elucidate the mechanisms responsible for the flow irreversibility and to determine the anatomical sites where the flow irreversibility originates, we analyzed color patterns of cross-sectional images taken sequentially over more than 10 different airway generations. We sought to identify whether characteristic lengths might be present, and if so, whether these lengths would indicate some particular depth in the airway tree. We used a spatial correlation analysis of the image pattern (32, 33). Each cross-sectional image was covered by M square boxes, each with an edge length E. For a given box size, let μ_i and $\bar{\mu}$ be the mean color intensity in the ith box and the overall mean intensity, respectively. We computed the standard deviation, SD, [$SD^2 = \Sigma(\mu_i - \bar{\mu})^2/M$] and coefficient of variation, $CV = SD/\bar{\mu}$ of the set of intensities μ_i. By changing E (and hence M), this procedure was repeated for box sizes spanning more than 5 orders of magnitude for each image.

This analysis resulted in two observations. First, all of the images analyzed showed a nearly linear relationship between log(CV) and (E^2) with a slope of about −0.1 (Fig. 2). This finding indicated that the mixing patterns were fractal with a fractal dimension $D = 1.1$ [$D = 1 - \partial\log(CV)/\partial\log(E^2)$] (32, 33). Second, the fractal nature of these mixing patterns appeared to be invariant throughout the tracheobronchial tree.

Time Evolution of Color (Mixing) Patterns. To quantify the extent of mixing in the acini, we examined the time evolution of color (mixing) patterns on the transverse cross sections of acinar airways (approximately 200 μ in diameter) at the end of either one, two, three, or four breathing cycles. After one cycle ($N = 1$, Fig. 3), most of the acinar airways appeared predominantly white, with microscopic traces of blue. After two or three cycles, however, a large amount of tidal (blue) fluid appeared on the cross-sectional images ($N = 2$, 3; Fig. 3), indicating that substantial net axial transport had

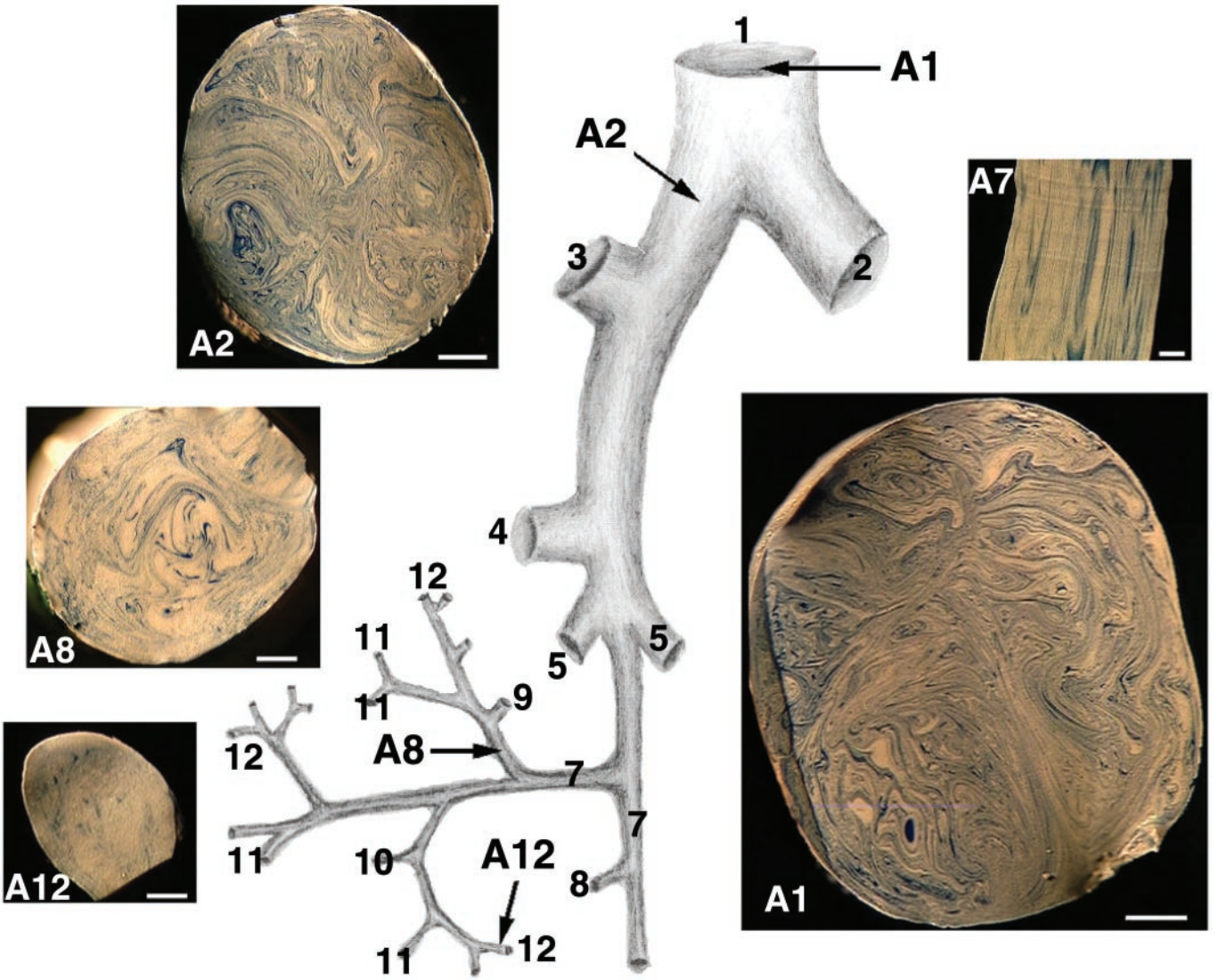

Fig. 1. Typical flow patterns observed on airway cross sections at different locations in the tracheobronchial tree after one ventilatory cycle. Images A1 (bar = 500 μm), A2 (bar = 500 μm), A8 (bar = 200 μm), and A12 (bar = 100 μm) show patterns on the transverse section of the trachea, the right main stem bronchus, a medium-size airway, and a small airway, respectively. Image A7 (bar = 100 μm) shows longitudinal section through a medium-size airway. Images shown are representative of five rat lungs analyzed.

occurred along the bronchial-acinar tree. The cross-sectional images of acinar airways showed clearly delineated interface patterns with both blue and white fluids being stretched and folded (discussed below). After four cycles, the clarity of the interface patterns had largely disappeared, and the previously clear blue/white patterns changed into smeared and mixed bluish-white uniformity ($N = 4$, Fig. 3).

Determination of Folding Factor. Convective folding of mixing patterns similar to the ones shown in Fig. 3, particularly at $N = 2, 3$, were consistently observed throughout the experiments. This finding suggests that there may be a specific cycle-by-cycle folding factor f, characteristic of the acinar duct structure. To test this notion, we analyzed the cross-sectional images of acinar airways for each of $N = 1, 2, 3$, and 4. Approximately 200 images (taken at $\times 80$ magnification) obtained from 12 animals (three animals for each cycle number) were randomly selected. For each image, we computed the characteristic distance between neighboring blue/white interfaces defined as the harmonic mean wavelength, l_w, obtained by two-dimensional spectral analysis. The time evolution of l_w, normalized by airway diameter, d, showed a sharp decrease from $N = 1$ to $N = 3$, reflecting the decreasing lateral length scales associated with folding. This was followed by a sudden increase in l_w/d at $N = 4$, caused by the diffusive loss of high-frequency components in the pattern. To determine the folding factor f in rat acini, we developed a simple convection/diffusion mathematical model with a parameterized folding factor and fit this to the data. The model represents a simple evolving sine wave convective pattern, whose wavelength is divided by a folding factor f for each breath cycle and whose amplitude is allowed to smooth out by diffusion. We found that a best fit to the data was obtained with a folding factor $f = 2.3$. The interpretation and significance of this value to the rapidity of convective mixing is discussed below.

Discussion

The principal findings of this study are that (*i*) the interaction between inhaled tidal fluid and residual alveolar fluid is not kinematically reversible even deep in the lungs under very low Reynolds number flow conditions. This kinematic irreversibility leads to the formation of complex (stretch and fold) convective

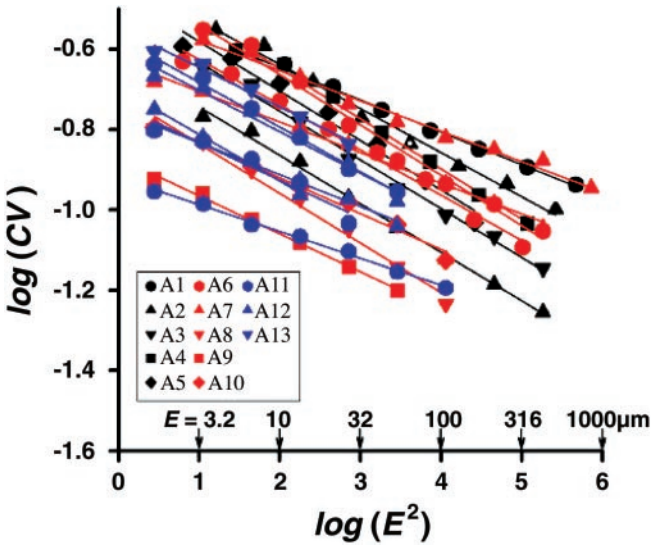

Fig. 2. Fractal analysis performed on color patterns of airway cross sections after one ventilatory cycle. *M* (*E*-by-*E*) squares covering most of the transverse cross-sectional area of each image were used for the analysis. Different-colored symbols show different airway generations, starting at the trachea to 12- to 13th-generation airways. Note that even though some images (e.g., A12 in Fig. 1) appeared mostly white because of the low color contrast (manifested in the low absolute value of the CV), the dependence of CV on E^2 nevertheless continued to show the same fractal pattern with $D = 1.1$. Images obtained from the two animals analyzed by this method were found to yield virtually identical results.

mixing patterns. (*ii*) The convoluted mixing patterns with a multitude of folds observed from the trachea to the 12- to 13th-generation airways are fractal with fractal dimension of ≈1.1. This consistent fractal dimension over many airway generations suggests that the origin of irreversibility is in the acinus, most likely originating from chaotic alveolar flow. The presence of alveolar recirculation (discussed below), together with our recent numerical studies (26–28), supports this idea. (*iii*) Image analysis on the temporal evolution of mixing patterns revealed

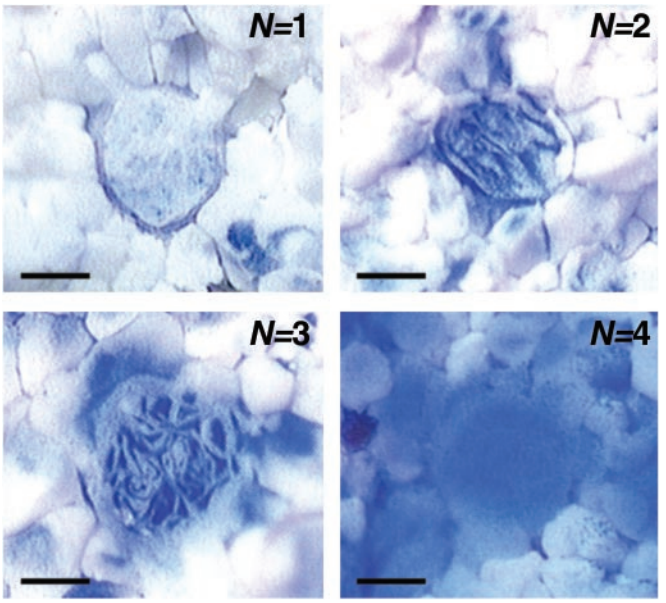

Fig. 3. Typical mixing pattern of two colors observed in approximately 200-μm acinar airways of adult rats after ventilatory cycles of $N = 1, 2, 3$, and 4. (Bars = 100 μm.)

that cycle-by-cycle convective folding is an important feature of acinar mixing, suggesting that, as described below, there can be a burst of acinar mixing that can occur within a few ventilatory cycles. Taken together, the results of these flow visualization studies suggest that the acinar mixing process for aerosols is radically different from any diffusive or dispersive process, previously the widely accepted mechanism in classical aerosol transport theories.

Mechanisms Responsible for the Observed Mixing. Flow visualization studies performed in excised rat lungs demonstrated convoluted stretch and fold mixing patterns on transverse cross sections of the airways throughout the tracheobronchial tree (Fig. 1). How could such a high degree of mixing occur as early as after only one ventilatory cycle? Two possibilities can be excluded. First, instabilities (e.g., Marangoni) associated with interfacial tension between the two fluids could possibly generate small scale mixing, but this is unlikely because, apart from the dye, the two fluids are identical. This was confirmed by the results of our control experiments. Second, if fluid inertia contributed significantly to mixing, we would have seen inertia-based secondary flows such as turbulent eddies or separation bubbles at airway bifurcations on longitudinal sections. We did not observe any sign of such complex mixing patterns.

The underlying mechanisms that we believe responsible for the observed mixing may be described as follows. During inspiration, as the lungs expand, the front of the tidal fluid represented by the interface of the blue/white colors also expands. Note that because of the fluid no-slip conditions, the perimeter of the blue/white interface remains in contact with the wall of the tracheal cannula. It follows that the color interface is enormously stretched by the end of the inspiration, entering multiple airway pathways where about 2^{23} distal acinar ducts (for human lungs; ref. 34) are connected to a single trachea sampling millions of alveolar spaces. At this point, however, little folding of the interface has taken place yet. This stretching of the color interface into the alveolar region by the end of inspiration was confirmed by the results of supplementary experiments. Data obtained at $N = ½$ (at the end of the first inspiration) show that most of the large, medium size, and alveolar airways were entirely filled with tidal (blue) fluid with no sign of significant mixing in the acini at the end of the first inspiration. However, many alveoli showed recirculation flow patterns (Fig. 4). This is important because it is now known that fluid particle trajectories can be chaotic in three-dimensional recirculating Stokes flows (35). Alveolar recirculation flows and their interplay with the driving oscillatory flows are likely to play a role in generating acinar flow irreversibility (see below in more detail); chaotic trajectories, specifically, occur where there is resonance between the external driving flow and the recirculation (36).

During expiration, the stretched color interface contracts, approximating the contraction of the lungs and emerging into the single trachea. Importantly, however, because of even minute levels of irreversibility in the nature of the flow fields (refs. 26–28 and 37–39; also see below), each fluid element does not retrace its original inspiratory path, but rather ends up at a place different from its initial position. The lack of any sign of interface breakup suggests that the observed blue/white interface patterns remain a simply connected surface that consists of a multitude of folds primarily in the axial direction. We suggest that the interface samples an extremely large number of parallel pathways during each breath, and that this, coupled with failure to preserve exact reversibility, results in the complex folding patterns we observed.

Fractal Patterns and Chaotic Mixing. We have previously studied particle motion produced by low Reynolds number flow in an axisymmetric model acinus, which expanded and contracted rhythmically (26–28, 39). Our numerical and experimental results show that this idealized model has features that can produce chaotic dynamics when the system is perturbed. Specifically, there is

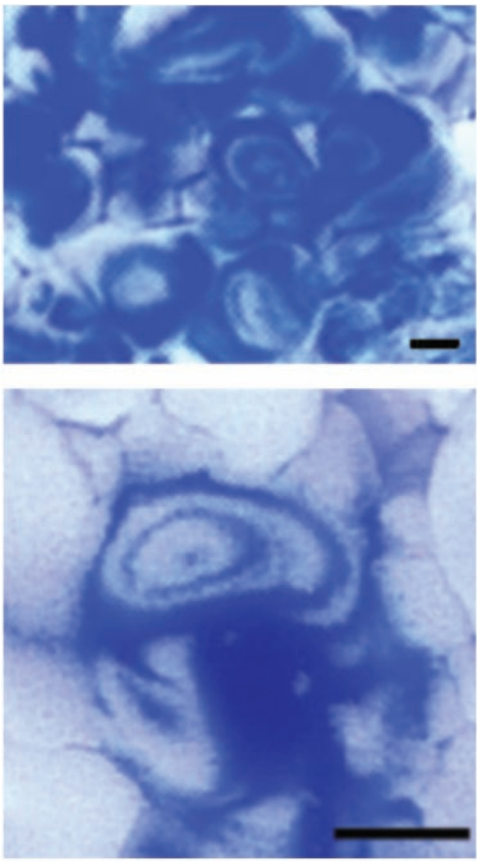

Fig. 4. Alveolar recirculation. In many alveoli, circular (or ellipsoidal) blue/white color patterns were observed at $N = 1/2$. (*Upper*) A field of multiple alveoli, each containing a recirculating pattern. (*Lower*) Enlarged view of an alveolar recirculation flow. (Bar = 100 μm.)

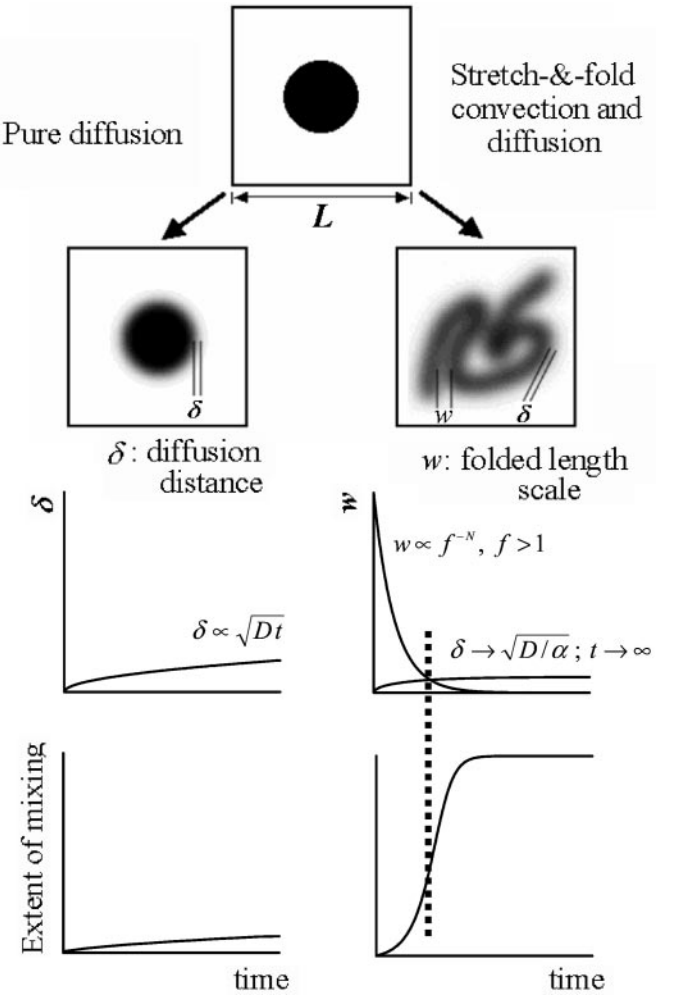

Fig. 5. Illustration comparing Brownian tracer mixing between a system with pure diffusion and a system with stretch and fold convection and diffusion. (*Top*) Schematic view of these two different systems. (*Middle Left*) The slowly increasing length scale for mixing (δ) in pure diffusion. (*Middle Right*) With stretch and fold convection, δ also increases slowly (but approaches an asymptotic value); by contrast, the folding length scale, *w*, decreases exponentially rapidly. (*Bottom*) Representation of the evolving extent of mixing corresponding to diffusion alone and to diffusion coupled with stretch and fold convection. At the time when the two length scales are comparable (vertical dotted line), there is sharp jump in mixing (entropy burst).

extensive recirculation within the alveolus (Fig. 4); the boundary of the recirculation region is a homoclinic orbit whose saddle point is situated away from the alveolar wall. Even small perturbations, such as nonzero Re (26, 28, 39), asynchrony (27, 38), or the lack of axisymmetry (35) make such flow nonintegrable (two fluid elements that are initially arbitrary close to one another become exponentially far apart). The stable and unstable manifolds are wildly tangled in phase space, which produces chaotic trajectories. It is also well known that iterated stretching and folding of fluid by a homoclinic tangle produces surfaces that have fractal geometry (32, 40), consistent with our observations (Fig. 1). Moreover, the fact that these observed fractal patterns persist over many generations with nearly the same fractal dimension $D = 1.1$ (Fig. 2) suggests that this mixing originates deep in the lung rather than in the central airways.

Mixing Burst. The temporal evolution of convection patterns observed in our study fundamentally differs from the one predicted by the classical theory based on kinematically reversible fluid flow. To illustrate this, consider the following two systems. One is kinematically reversible (Fig. 5 *Left*) and the other has irreversible stretch and fold convection (Fig. 5 *Right*). We introduce a Brownian tracer into both systems and track the evolution of diffusive and convective length scales in both systems. In the kinematically reversible system, there is no net convective transport; mixing is therefore characterized by a diffusion distance δ, which increases slowly with time *t,* typically like $\sqrt{Dt}$, where *D* is the tracer diffusivity (Fig. 5 *Middle Left*). Significant mixing only occurs when δ becomes of the order of *L*, the fixed system size, which in our case is a typical alveolar dimension (a few hundred microns; ref. 16). For fine aerosol particles, this process would be very slow (Fig. 5 *Bottom Left*) because of the low diffusivities (e.g., the diffusivity of typical 0.5-μ aerosol particles is around 10^{-7} cm^2/s, 5 or 6 orders of magnitude smaller than the diffusivities of O_2 or CO_2 gas molecules). By contrast, in the system with stretch and fold convection, diffusion and convection interact. The diffusion length scale δ initially increases as $\sqrt{Dt}$, but asymptotically approaches $\sqrt{D/\alpha}$, where α is the stretching rate. Importantly, however, the length scale over which diffusion must operate to effect mixing is no longer fixed at the system size *L*, but because of convective folding, decreases exponentially with cycle number *N*. This can be expressed as f^{-N}, where *f* is a characteristic cycle-by-cycle folding factor (Fig. 5 *Middle Right*). In this interaction, mixing is initially very slow, but suddenly increases after a few cycles when the rapidly decreasing folded scales $L\ f^{-N}$ become comparable to the asymptotically constant value of diffusion length scale δ (Fig. 5 *Bottom Right*). This phenomenon—a sudden increase in mixing that can be described by

an equivalent entropy burst (37)—is a characteristic feature of chaotic mixing (29) and is quantified by the folding factor f. In rat acinar airways with diameter of approximately 200 μm, the folding factor f was about 2.3, which means that the lateral length scales over which the complexity of the convective flow patterns is evolving are decreased by more than half at every breath. Equivalently, the complexity of the pattern itself more than doubles each breath. This is an exponentiating phenomenon, which in consequence implies that only a modest number of breaths are required to ensure that these mixing lengths become sufficiently small that true diffusive and irreversible mixing can take place, even for very low diffusible aerosols.

Summary. Although acinar flow patterns likely have little effect on the gas exchange processes of highly diffusible respiratory gasses (O_2 and CO_2), they play an important role in determining the fate of inhaled fine particles with low diffusivity and little gravitational sedimentation. In this study, direct observations of flow patterns were made in fresh excised lungs and revealed that low Reynolds number acinar flows are neither simple nor reversible. Instead, they exhibit stretch and fold patterns, characteristic of chaotic flow (29). This finding suggests that aerosol transport and deposition in the pulmonary acinus are governed by entirely different dynamics than processes (17–21) based on reversible flows, and cannot be described by dispersions based on effective diffusivities. We conclude that chaotic acinar flow may be the origin of substantial mixing and transport of fine aerosols deep in the lung.

We thank D. Mazzucco and Prof. G. McKinley of Polymer Fluid Laboratory, Massachusetts Institute of Technology for characterizing Microfil silicone fluid and J. Roberts, J. E. Rogers, and J. Lai for technical assistance. This work was supported by National Heart, Lung, and Blood Institution Grant HL-54885, and in part, by Environmental Protection Agency Research Award R827353.

1. Smith, K. R. (2000) *Proc. Natl. Acad. Sci. USA* **97,** 13286–13293.
2. Pyne, S. (2002) *Science* **295,** 1994.
3. Beckett, W. S. (2000) *N. Engl. J. Med.* **342,** 406–413.
4. Iribarren, C., Tekawa, I. S., Sidney, S. & Friedman, G. D. (1999) *N. Engl. J. Med.* **340,** 1773–1780.
5. Goldman, D. A. (2000) *Pediatr. Infect. Dis. J.* **19,** S97–S102.
6. Peters, C. J. & Hartley, D. M. (2002) *Lancet* **359,** 710–711.
7. Swartz, M. N. (2001) *N. Engl. J. Med.* **345,** 1621–1626.
8. Small, P. M. & Fujiwara, P. I. (2001) *N. Engl. J. Med.* **345,** 189–200.
9. Dockery, D. W., Pope, C. A., III, Xu, X., Spengler, J. D., Ware, J. H., Fay, M. E., Ferris, B. G., Jr., & Speizer, F. E. (1993) *N. Engl. J. Med.* **329,** 1753–1759.
10. Brunekreef, B. (1997) *Occup. Environ. Med.* **54,** 781–784.
11. Cairns, J. (1979) *Cancer: Science and Society* (Freeman, San Francisco, CA).
12. Pedley, T. J., Schroter, R. C. & Sudlow, M. F. (1977) in *Bioengineering Aspects of the Lung*, ed. West, J. B. (Dekker, New York), pp. 163–265.
13. Ardila, R., Horie, T. & Hildebrandt, J. (1974) *Respir. Physiol.* **20,** 105–115.
14. Gil, J., Bachofen, H., Gehr, P. & Weibel, E. R. (1979) *J. Appl. Physiol.* **45,** 990–1001.
15. Miki, H., Butler, J. P., Rogers, R. A. & Lehr, J. (1993) *J. Appl. Physiol.* **75,** 1630–1636.
16. Weibel, E. R. (1986) in *Handbook of Physiology: The Respiratory System*, ed. Fishman, A. P. (Am. Physiol. Soc., Bethesda), pp. 89–111.
17. Davidson, M. R. & Fitz-Gerald, J. M. (1972) *J. Fluid Mech.* **52,** 161–177.
18. Davies, C. N. (1972) *J. Appl. Physiol.* **32,** 601–611.
19. Watson, E. J. (1974) *J. Appl. Physiol.* **37,** 251 (appendix).
20. Ultman, J. S. (1985) in *Gas Mixing and Distribution in the Lung*, eds. Engel, L. A. & Paiva, M. (Dekker, New York), pp. 63–163.
21. West, J. B. (1995) *Respiratory Physiology: The Essentials* (William & Wilkins, Baltimore).
22. Taylor, G. I. (1960) *Low Reynolds Number Flow* (Educational Services, Newton, MA), 16-mm film.
23. Heyder, J., Blanchard, J. D., Feldman, H. A. & Brain, J. D. (1988) *J. Appl. Physiol.* **64,** 1273–1278.
24. Schulz, H., Heilmann, P., Hillebrecht, A., Gebhart, J., Meyer, M., Piiper, J. & Heyder. J. (1992) *J. Appl. Physiol.* **72,** 1557–1562.
25. Darquenne, C., Paiva, M., West, J. B. & Prisk, G. K. (1997) *J. Appl. Physiol.* **83,** 2029–2036.
26. Tsuda, A., Henry, F. S. & Butler, J. P. (1995) *J. Appl. Physiol.* **79,** 1055–1063.
27. Haber, S., Butler, J. P., Brenner, H., Emanuel, I. & Tsuda, A. (2000) *J. Fluid Mech.* **405,** 243–268.
28. Henry, F. S., Butler, J. P. & Tsuda, A. (2002) *J. Appl. Physiol.* **92,** 835–845.
29. Ottino, J. M. (1989) *The Kinematics of Mixing: Stretching, Chaos, and Transport* (Cambridge Univ. Press, Cambridge, U.K.).
30. Aref, H. (1984) *J. Fluid Mech.* **143,** 1–21.
31. Ottino, J. M., Leong, C. W., Rising, H. & Swanson, P. D. (1988) *Nature (London)* **333,** 419–425.
32. Sommerer, J. C. (1994) *Physica* D **76,** 85–98.
33. Bassingthwaighte, J. J., Liebovitch, L. S. & West, B. J. (1994) *Fractal Physiology* (Oxford Univ. Press, Oxford).
34. Weibel, E. R. & Gomez, D. M. (1962) *Science* **137,** 577–585.
35. Bajer, K. & Moffatt, H. K. (1990) *J. Fluid Mech.* **212,** 337–364.
36. Hydon, P. E. (1994) *Physica D* **76,** 44–54.
37. Butler, J. P. & Tsuda, A. (1997) *J. Appl. Physiol.* **83,** 800–809.
38. Tsuda, A., Otani, Y. & Butler, J. P. (1999) *J. Appl. Physiol.* **86,** 977–984.
39. Tippe, A. & Tsuda, A. (2000) *J. Aerosol Sci.* **31,** 979–986.
40. Mandelbrot, B. B. (1982) *The Fractal Geometry of Nature* (Freeman, San Francisco).